Classical trajectory treatment of inelastic scattering in collisions of H^+ with H_2, HD, and D_2 †

Clayton F. Giese
Tate Laboratory of Physics, School of Physics and Astronomy, University of Minnesota, Minneapolis, Minnesota 55455

W. Ronald Gentry
Chemical Dynamics Laboratory, Department of Chemistry, University of Minnesota, Minneapolis, Minnesota 55455
(Received 29 July 1974)

A semiclassical model for vibrational excitation in molecular collisions is proposed, in which three-dimensional classical trajectory calculations are used to evaluate the quantum vibrational transition probabilities. Using an accurate analytic fit to 138 *ab initio* points in the important region of the H_3^+ potential surface and a new Monte Carlo interpolation method for averaging over initial conditions, we apply the model to vibrational excitation in collisions of H^+ with H_2, HD, and D_2. The calculations reveal the necessity of correcting our previously reported experimental vibrational transition probabilities for rotational contributions. Once this is done, the experimental data and the model calculations are in very good agreement. The theoretical results support our previous conclusion that vibrational excitation in this system is caused primarily by dilution of the molecular bond by the passing proton. The observed maximum in the experimental inelastic differential cross sections at approximately half the rainbow angle is shown to be associated with the second classical rainbow, which results from the anisotropy of the potential.

INTRODUCTION

In a previous paper,[1] we reported experimental measurements of the quantum transition probabilities and differential cross sections for the excitation of resolved vibrational states in nonreactive collisions of H^+ with H_2, HD, and D_2. These experiments spanned the range of initial relative kinetic energy from 4 to 21 eV and the range of center-of-mass (c.m.) scattering angle from about 5° to slightly beyond the rainbow angle for a given energy. From qualitative considerations involving the shape of the H_3^+ potential-energy hypersurface, the large magnitude of the vibrational excitation probabilities at small scattering angles, and the observed isotope effects, we concluded that the principal mechanism for vibrational excitation in this system is an effect which we called "bond dilution"—the temporary withdrawal of electron density from the molecular bond by the passing proton. In this picture, the vibrational excitation is caused by a stretching force which acts simultaneously on both of the H_2 nuclei. This mechanism is quite different from those theories of vibrational excitation in which the incident atom interacts directly only with the nearest atom of the molecule. Here we present a theoretical treatment of the collision dynamics in the energy and scattering angle regime of the experiments. The calculations confirm our original point of view regarding the mechanism of vibrational excitation in this system and also illuminate some features of the experimental data not previously understood.

The $H^+ + H_2$ system is a highly propitious one for comparison of theory and experiment since there is little averaging to be performed over experimental parameters. In the experiments a structureless particle collides with a molecule in a well-defined quantum state ($n = 0; J = 0, 1$) leading to scattering at a specific angle into a resolved molecular vibrational state with the rotational state probably unchanged. Also, the H_3^+ potential-energy hypersurface has been calculated accurately for a large number of configurations in the region of interest.

Progress in the theoretical treatment of vibrational excitation in molecular collisions has been reviewed recently by Secrest,[2] and earlier by Rapp and Kassal,[3] and by Takayanagi.[4] A wide variety of methods have been employed, including fully classical, fully quantum-mechanical, and many different semiclassical (or semiquantal) schemes. Although complete quantum-mechanical close-coupling calculations in three dimensions are now within the state of the art for some three-atom systems,[5] we have chosen instead to use a semiclassical model which provides a particularly graphic description of the vibrational excitation process.

The utility of semiclassical methods for molecular scattering problems is widely appreciated, not only for the savings in computational effort which are usually realized, but also for the physical insight which knowledge of the classical motion often makes possible. There are essentially two approaches to the application of classical mechanics

to the dynamics of inelastic and reactive scattering of molecules, corresponding to whether the boundary conditions employed are classical or quantal. Both have been applied to vibrational excitation in molecular collisions.[2] In the conventional semiclassical approach, those degrees of freedom in which the quantum numbers are large (usually those which are asymptotically translational) are treated classically, while those with small quantum numbers are treated quantum mechanically. Any classically allowed values of the initial and final dynamical variables are permitted for the classical motion. This procedure results in a set of coupled differential equations[3] (for example, Hamilton's equations coupled through the potential energy to the time-dependent Schrödinger equation) which, for a specified set of initial conditions, permit either direct numerical integration or the use of approximate solutions for the classical motion, the quantal motion, or both.

Recent theories of vibrational excitation formulated along these lines include those of Locker and Wilson,[6] Wartell and Cross,[7] Pechukas and Davis,[8] Penner and Wallace,[9] Ritchie,[10] and the "string-plucking" model of Gordon and Kuppermann.[11] A semiclassical treatment of the $H^+ + H_2$ system using an approximate potential was recently reported by Collins, Preston, and Cross.[12]

An alternative approach, recently developed by Miller and Marcus, is to use the classical equations of motion for all degrees of freedom, but to permit only those solutions which satisfy quantal boundary conditions.[13] This method is sometimes called "semiquantal"[2] to distinguish it from the more common semiclassical approximations. For vibrational excitation, it is required that the classical action in the vibrational mode have only quantally allowed values both initially and finally. This requires an iterative search of initial parameter space to find all classical paths (complex and real) which couple the desired initial and final states. No great problem arises in the case of a collinear atom-diatom collision, because only the initial phase angle of the oscillator must be varied to find the required solutions. For a meaningful comparison with experiment, however, a three-dimensional calculation is needed; therefore a simultaneous search of several variables must be performed to find all classical paths leading to the specified vibrational state, rotational state, and scattering angle. Such a treatment would be computationally formidable. A practical alternative recently suggested by Doll and Miller[14] is to treat only the vibrational degree of freedom semiquantally, performing a classical average over the coordinates and momenta of all other degrees of freedom. This approximation is in the spirit of the semiclassical approach, in that those degrees of freedom in which the energy-level spacings are small are treated by conventional classical mechanics, while the semiquantal double-ended boundary conditions are applied only to the vibrational motion. The advantage this method has over the usual semiclassical approach is that only classical equations of motion need be solved. In general, however, there are important contributions to the cross section in this method from "classically forbidden" trajectories—those which are analytically continued through complex coordinate space. This makes the intuitive appeal of a classical description somewhat less than it otherwise would be.

The model which we propose here is an extension of some previous theories of vibrational excitation which exploit the very special relationship between the classical and quantum-mechanical equations of motion for a harmonic oscillator subject to a time-dependent force. Operationally, the model is very simple. For each set of initial conditions (translational energy, impact parameter, and molecular orientation) the exact three-dimensional classical trajectory is calculated for an initially stationary oscillator. The final vibrational energy acquired by the molecule is used to determine the quantum vibrational transition probabilities according to a semiclassical prescription. The transition probabilities for individual collisions are then averaged over initial conditions by a Monte Carlo treatment. We call our method the DECENT model, for *d*istribution (among quantum states) of *e*xact *c*lassical *en*ergy *t*ransfer.

Unlike the method of Doll and Miller,[14] the DECENT model is appropriate for the semiclassical treatment of vibrational transitions only. For this special class of scattering problems, however, it has several distinct advantages. As in a semiquantal formulation, the dynamical equations which are solved are solely those of classical mechanics. The DECENT approximation, however, requires the calculation of only real trajectories, even for the treatment of classically forbidden transitions. It also uses classical boundary conditions, but obviates the necessity of averaging over the initial vibrational phase.

DECENT MODEL

Our starting point is the harmonic-oscillator problem. The special relationship which exists between the classical and quantum-mechanical descriptions of simple harmonic motion is a familiar textbook example.[15] The result may be viewed as a manifestation of the Ehrenfest theorem.

Consider the one-dimensional classical motion of a body of mass M subject to a force F. The

Newtonian equation of motion is

$$F(x)=M\frac{d^2x}{dt^2}, \tag{1}$$

which may be solved for the classical coordinate $x_c(t)$. The Ehrenfest theorem gives the corresponding relation for the quantum-mechanical average values of F and x:

$$\langle F(x)\rangle = M\frac{d^2\langle x\rangle}{dt^2}. \tag{2}$$

Ordinarily, one must first solve the appropriate Schrödinger equation to obtain the wave functions required for the evaluation of $\langle F\rangle$, in order to made use of Eq. (2). For the special case of a force function which is linear in x, however,

$$F(x)=a+bx, \tag{3}$$

the average value of the force is given by

$$\langle F(x)\rangle = \int_{-\infty}^{\infty}\psi^* F\psi\, dx = a+b\langle x\rangle; \tag{4}$$

therefore the average force quantum mechanically is simply the classical force evaluated at $\langle x\rangle$:

$$\langle F(x)\rangle = F(\langle x\rangle). \tag{5}$$

The Ehrenfest relation, Eq. (2), therefore shows that $\langle x\rangle$, the quantum-mechanical average value of x, obeys exactly the classical equations of motion.[16] This is the basis for the oscillating-wave-packet description of a simple harmonic oscillator. It can be shown that a minimum wave packet which is described by Gaussian distributions in position and momentum initially, when subjected to the harmonic oscillator Hamiltonian, does not spread with time and remains centered exactly at the same value of the coordinate obtained by solving the corresponding classical equation.[15] If the classical vibrational energy $\mathcal{E}$ is zero, the wave packet describes the (stationary) ground state of the harmonic oscillator, with energy $\frac{1}{2}\hbar\omega$. For any nonzero classical energy, the wave packet oscillates sinusoidally with the classical motion. An expansion of the nonstationary wave packet in terms of the stationary states of the harmonic-oscillator Hamiltonian gives a Poisson distribution for the probability of finding the system in a particular vibrational state n:

$$P_n=\epsilon^n e^{-\epsilon}/n!, \tag{6}$$

in which

$$\epsilon=\mathcal{E}/\hbar\omega \tag{7}$$

is the classical energy in units of the vibrational quantum. The quantum-mechanical average energy is $\mathcal{E}+\frac{1}{2}\hbar\omega$.

Now consider the motion of a particle subject not only to the harmonic-oscillator potential $\frac{1}{2}kx^2$, but also to an arbitrary time-dependent potential $U(x, t)$, which may be regarded as externally applied. In a collision, $U(x, t)$ is the potential which couples the vibrational motion to motion in the remaining coordinates. It can be calculated only by simultaneous solution of the equations of motion in all degrees of freedom. To solve the classical equations of motion for the perturbed oscillator, the external force $-\partial U/\partial x$ must be known (at any instant) at only one value of x, x_c, while quantum mechanically the force must be known for all values of x, since the wave function extends indefinitely. If $U(x, t)$ is expanded in a Maclaurin series, and the series truncated at the term linear in x, however, the classical and quantal problems are perfectly equivalent, since the external force is independent of x. The resulting potential

$$V(x, t)=\tfrac{1}{2}kx^2+U(0, t)-xF(t) \tag{8}$$

differs from the unperturbed potential only in having the position of its minimum shifted with an arbitrary time dependence determined by $F(t)$. The term $U(0, t)$, having no x dependence, cannot contribute to vibrational excitation and may be dropped.[3] Classically, the motion of the particle may be obtained by solving the equation

$$M\frac{d^2x}{dt^2}+kx=F(t). \tag{9}$$

The energy gained by an initially stationary classical oscillator is identical to the energy transferred to a nonstationary oscillator averaged over the initial vibrational phase,[4] and can be expressed in terms of the Fourier transform of the force at the harmonic oscillator frequency,[17]

$$\mathcal{E}=\frac{1}{2M}\left|\int_{-\infty}^{\infty}F(t)e^{-i\omega t}\,dt\right|^2. \tag{10}$$

The quantum-mechanical problem for the potential of Eq. (8) has been solved many times in various formulations.[18,19] For our purposes here, we need only the transition probabilities to all excited states from the initial state $n=0$. The result may be deduced immediately from the discussion given above. It is necessary only to note that the potential of Eq. (8) satisfies the required condition that $\langle x\rangle$ obey the classical equations of motion. The quantum-mechanical wave packet representing the ground state of the oscillator initially (with $\langle x\rangle=0$, $\langle p\rangle=0$), when subjected to the external potential $xF(t)$, responds exactly as a classical oscillator driven by the force $F(t)$ would respond. The wave packet does not distort and remains centered exactly on the value of x_c obtained by solving Eq. (9) with the initial boundary conditions appropriate for the quantum ground state, namely, $x_c=0$, (dx_c/dt)

$=0$. After the external force has decayed to zero the wave packet continues to oscillate with the classical motion on the original harmonic-oscillator potential; therefore the probability distribution for final vibrational states n is just that already given in Eq. (6)—a Poisson distribution with the average value $\epsilon = \mathcal{E}/\hbar\omega$.

By direct solution of the time-dependent Schrödinger equation with the potential of Eq. (8), Kerner[18] showed that the transition probabilities between any pair of initial and final states can in fact be specified in terms of the classical energy transfer to an initially stationary oscillator.[20] The essence of the DECENT model is that the semiclassical quantum transition probabilities, for the special case of a harmonic oscillator subject to an interaction potential which is of first order in the vibrational coordinate, can be calculated exactly using only classical mechanics for all degrees of freedom; i.e., by calculating the classical trajectory.

It is common in classical-trajectory treatments of reactive and inelastic scattering to give each ground-state molecule initially a classical vibrational energy equal to the quantum-mechanical zero-point energy, with a random initial phase. In the spirit of the semiclassical DECENT model, however, in which the classical value of the oscillator coordinate is to be interpreted as the center of the quantal wave packet, the classical trajectory should always be calculated with zero initial vibrational energy in the molecule, since a wave packet which is oscillating in time represents not a single eigenstate, but a superposition of many vibrational states. This observation is highly serendipitous, since a great deal of computer time is saved by eliminating the necessity for averaging over initial vibrational phase.

The DECENT model may easily be applied to vibrational excitation of polyatomic molecules by partitioning the final classical vibrational energy among all the normal modes ($\mathcal{E} = \sum \hbar\omega_i \epsilon_i$) and calculating the transition probabilities for each normal mode from Eq. (6), using the appropriate values of ω_i and ϵ_i.[21]

There are two approximations involved in the DECENT model: (i) the use of classical mechanics for the translational and rotational motion, and (ii) the use of vibrational transition probabilities appropriate for a harmonic oscillator driven by a perturbation potential linear in the vibrational coordinate. Since the translational energy required for vibrational excitation is at least as large as a vibrational quantum, the first approximation should generally be a good one. Quantum details of the angular distribution, such as the shape of the rainbow maximum and the small-angle interference structure, will, of course, not be predicted correctly; however, the agreement between the classical and quantal differential cross sections should be somewhat better than in the case of scattering from a spherical potential, since averaging over orientation of an anisotropic potential will tend to remove the classical rainbow infinity and decrease the amplitude of the quantum interferences.[22] The second approximation has been considered by Treanor,[23] who used the time-dependent eigenfunctions which result from the linear forcing potential as the basis for a perturbation calculation, to show the effect of higher-order terms in the potential. Without solving either the classical or quantal problems explicitly Treanor demonstrated that the *difference* between the two results is small, even for very nonlinear potentials. The classical vibrational energy used in the DECENT model is therefore the exact value obtained using the real potential-energy surface, rather than a harmonic-oscillator approximation to the molecular potential.

The DECENT approximation will not be valid for cases in which the average vibrational-energy transfer is not the same classically and quantally. Since the average energy transfer to an oscillator from a time-dependent force is always positive, this model cannot be applied to deexcitation of vibrationally excited molecules in slow collisions.[24]

Another limitation of the DECENT model is that energy is conserved only on the average. A single classical trajectory, with particular initial and final translational energies, is used to calculate probabilities for all final vibrational states. Although there is no problem if the vibrational-energy transfer is much smaller than the initial translational energy, for collisions in which a large fraction of the total available energy is transferred into vibration, the distribution of Eq. (6) will give significant probability for transition to energetically inaccessible states. A suitable *ad hoc* modification for treating such cases might be to replace Eq. (6) with the "binominal" probability distribution

$$P_n = \frac{N!}{n!\,(N-n)!}\, p^n (1-p)^{N-n}, \tag{11}$$

where N is the total number of vibrational states energetically accessible and p is defined by

$$\epsilon = Np\,. \tag{12}$$

For large N, Eq. (11) goes over smoothly to the Poisson distribution. Equation (11) allows no excitation to inaccessible states while preserving a quantum state distribution with an average vibrational energy equal to the classical value. For $\epsilon \ll N$, Eqs. (6) and (11) give essentially the same

probabilities. In all the calculations reported here, the simpler formula, Eq. (6), was used.

Previous theories of vibrational excitation which make use of the correspondence between the classical and quantal forced-oscillator results include the oriented-nonlinear-encounter model of Shin,[25] and two collinear treatments—the CEFQO (classical-energy forced quantum oscillator) model of Holdy, Klotz, and Wilson,[26] and the ITFITS (improvement to forced oscillator—impulsive transfer semiclassical) approximation of Heidrich, Wilson, and Rapp.[27] The ITFITS scheme was generalized by Morse[28] to three-dimensional collisions on a spherically symmetric potential. Because of either a dynamical approximation[29] or an assumed functional form for the potential which is not suitable in this case, none of these models appeared to provide a reasonable basis for comparison with experiment in the $H^+ + H_2$ system.

METHOD

The calculations reported here were done in three parts: The choice of an analytic representation of the H_3^+ potential-energy hypersurface, the calculation of classical trajectories on this surface for a grid of initial collision parameters, and the averaging over initial conditions by a Monte Carlo interpolation method.

Interaction potential

We performed early tests of the classical-trajectory program using a potential calculated by the semiempirical diatomics-in-molecules method.[30] However, we found that the results were so sensitive to the shape of the potential surface that the most accurate possible determination of that shape was essential for a meaningful comparison with experiment. Three sets of *ab initio* calculations for the ground-state H_3^+ potential were available: (i) 249 points, over a comprehensive set of coordinates, by Csizmadia *et al.*[31] (ii) 85 points, all for the isosceles configuration, by Bauschlicher *et al.*,[32] and (iii) 69 points by Carney and Porter.[33]

The H_3^+ ground-state surface, for $r \sim 2.5$ bohr, has an avoided crossing with a surface which asymptotically corresponds to $H_2^+ + H$.[30,32] For large R, this change in character is sharp, and to represent the ground-state surface one would need to use functions for the analytic representation capable of providing an abrupt change in slope at $r \sim 2.5$. However, for large R the electronic transition probability is high and diabatic behavior is expected, meaning that the appropriate potential is one which continues smoothly through the crossing. As R becomes small, the transition probability decreases, leading to adiabatic behavior, but also the change in slope becomes much less abrupt. Accordingly, we have used an analytic representation for the potential which does not produce any seam at $r \sim 2.5$. In fitting our function to the calculated potential values, we used points only for r values $\lesssim 2.5$ bohr, because very few collisions in this study explore regions beyond $r \sim 2.5$ bohr. For those collisions which do, the extrapolation of our potential to $r > 2.5$ bohr will provide a reasonable approximation to the true potential.

We found it possible to fit analytic representations of the potential to the values from all three sets of *ab initio* calculations simultaneously, using an iterative least-squares fitting program. However, calculation (iii) was done mainly for a set of minute distortions of the equilateral configuration and a set of large distortions, with a few points in between. Calculation (ii) displayed systematic differences from a smooth surface fitted to calculation (i). These differences were not very large (≤ 0.0056 hartree for $r \geq 1.2$ bohr), but could not be removed without considerably worsening the fit to the points of calculation (i). It was our judgment that an analytic fit to a restricted set of results from calculation (i) alone, suitably adjusted, was the best representation of the H_3^+ potential surface for the purposes of this calculation.

Adjustments of the ab initio calculations

Comparisons of the H_3^+ potential calculations from (i) with the best estimates[31] of these authors for the equilateral minimum, the collinear minimum, and the potential for large R reveal the calculated potential to be high by 0.0047, 0.0069, and 0.0077 hartree, respectively. We therefore adjusted the calculated points using the following correction formula, which forces the surface to agree with the best estimates of the real potential at these three configurations and varies smoothly over the whole surface:

$$V_{\text{corr}} = V_{\text{calc}} - 0.0057 - 0.00134 P_2(1 - F_0) - 0.00223 F_0, \tag{13}$$

where $F_0 = R^4/(100 + R^4)$ and $P_2 = 0.5[3\cos^2(\alpha) - 1]$. $\vec{R}$ is the vector from the H_2 center of mass to the proton and α is the angle between this vector and the H_2 internuclear axis. All numerical values are given in atomic units.

Since for large R we felt that the interaction potential was more accurately represented by the charge-induced dipole and charge-quadrupole contributions,[34,35] we discarded the potential points calculated for $R > 6$ bohr, along with those for $r > 2.5$ bohr. This left 138 points on the surface to be fitted to our analytic form.

Analytic potential

After considerable experimentation, the following ten-parameter analytic function evolved. All ten parameters (underlined) were optimized by an iterative least-squares fit of this function to the 138 calculated points.[36]

Let us call the three interatomic distances $R_k (k=1,2,3)$, with R_2 the distance between the two nuclei of H_2 (thus $R_2 = r$). Then the potential V in atomic units is given by

$$V = \sum_{k=1}^{3} H(R_k) + PF_1 + QF_2 + \underline{0.073225} F_3 + 0.17449 . \tag{14}$$

$H(R_k)$ is a minor variant of a Hulburt-Hirschfelder potential function[37]:

$$H(R_k) = A[-2E + E^2 - 0.1145 Z^3 E^2 (1-Z)], \tag{15}$$

where

$$E = e^{-Z}$$

$$Z = B(R_k/R_e - 1),$$

$$B = 1.4426 - \underline{0.12871} F_4,$$

$$R_e = 1.40083 + \underline{0.27923} F_4,$$

$$A = 0.17449 - (\underline{0.014665} + \underline{0.022721} R_k) F_4,$$

and P is the charge-induced dipole contribution

$$P = -(A_0 + A_2 P_2) R^{-4} .$$

A_0 and A_2 are determined from cubic fits to the spherical and angle-dependent polarizabilities versus R_2 as calculated by Kolos and Wolniewicz.[34] The numerical values are

$$A_0 = 2.6091 + [2.246 + (0.3181 - 0.1194\rho)\rho]\rho ,$$

$$A_2 = 0.60735 + [1.3586 + (0.5573 - 0.3170\rho)\rho]\rho ,$$

where $\rho = R_2 - 1.40083$. The charge-quadrupole contribution Q is given by $Q = Q_2 P_2 R^{-3}$, where Q_2 is determined from a cubic fit to the quadrupole moment versus R_2,[35]

$$Q_2 = 0.45886 + [0.53223 + (0.03234 - 0.091474\rho)\rho]\rho .$$

Finally, F_1, F_2, F_3, F_4 are roll-off and roll-on functions:

$$F_1 = R^5/(\underline{133.6729} + R^5),$$

$$F_2 = R^4/(\underline{29.6088} + R^4),$$

$$F_3 = 1/\{1 + \exp[\underline{2.1135}(R - \underline{2.4421})]\},$$

$$F_4 = 1/(1 + \underline{0.000164189} R^6).$$

The heart of this analytic representation is the sum over diatomic potential functions $H(R_k)$, in which the width, depth, and position of minimum are allowed to vary from the values for H_2, as the proton approaches. This form was suggested by the success of the diatomics-in-molecules calculation in representing the general shape of the surface. It has the advantages of ensuring the continuity of the potential surface and its derivatives and of passing correctly to an accurate H_2 potential function at large proton distances.

Comparison with ab initio calculations

The potential function [Eq. (14)], compared with the set of 138 points which were fitted, has a standard error of 0.00062 hartree, with a maximum difference of 0.0030 hartree.

The standard error for the comparison with the calculations of Carney and Porter[33] is minimized when their points are lowered by 0.0069 hartree. When this is done, some large differences persist, by far the worst being for $\alpha = 90°$, $r = 0.33$ bohr, $R = 2.58$ bohr, at which the Carney-Porter calculation is 0.704 hartree higher than our function. However, when r and R are restricted to values greater than 0.9 bohr, eliminating 11 points, the standard error is 0.0039 hartree, with a maximum difference of 0.015 hartree.

Comparison of our potential function with the 32 points calculated by Bauschlicher *et al.*,[32] for configurations with $R \leq 8.0$ bohr, $r \leq 2.4$ bohr, reveals our surface to be lower than their calculation by an average of 0.0025 hartree, with a standard error of 0.0033 hartree. The largest deviation is at $r = 1.00$ bohr, $R = 2.06$ bohr, where their calculation is higher by 0.013 hartree.

Some salient features of the potential and its derivatives

Figure 1 displays contour maps of the potential $V(R, r, \alpha)$ and the stretching force $-\partial V/\partial r$ versus R and α, for r fixed at 1.40083 bohr. The potential contours are very nearly spherical for $R > 2.5$ bohr, indicating that the long-range torque on the molecule is small.

The stretching force is positive everywhere for $R > 2$ bohr and reaches its maximum value at $\alpha = 0°$, not 90° where the potential is deepest. This force is effective at much longer range than the potential itself. Notice that at $R \sim 5$ bohr the potential is less than one-tenth of its value at the minimum, while the force is about one-half its maximum value.

Figure 2 shows for isosceles and collinear configurations how the equilibrium H_2 separation and the force constant vary with R. The effects of "bond dilution" in this system are striking. As the proton approaches to ~3 bohr, the equilibrium distance increases by ~20% and the force constant decreases by a factor of ~2, compared to an isolated H_2 molecule. The enhancement of the vibrational excitation process by the large changes in r_e and k

for this system was anticipated by Korobkin and Slawsky.[38] Similar features of the potential surface could be related to the " ballistic" mechanism for inelastic scattering suggested by Loesch and Herschbach.[39]

Trajectory calculations on a (b,θ,ϕ) grid

The collision trajectories are calculated in a Cartesian coordinate system, with the proton initially traveling parallel to the z axis at $x=b, y=0$ and the initial molecular orientation specified by the polar angle θ relative to the z axis and the azimuthal angle ϕ relative to the xz plane. The initial vibrational energy is required by the rationale of the DECENT model to be taken as zero. Since the duration of a collision in this energy regime is much smaller than a molecular rotational period, the initial rotational angular momentum was also assumed to be zero, making the trajectory at a given kinetic energy a function only of the three parameters b, θ, and ϕ. The collision results of interest (the total molecular internal energy and rotational angular momentum, and the polar scattering angle χ) can therefore each be considered as a hypersurface in (b, θ, ϕ) space. Although very complicated in form, these surfaces were found to be sufficiently smooth to be accurately represented by a practicable grid in initial parameters.

In all cases, ϕ was gridded from 0° to 180° with a spacing of 15° (13 values), and $\cos\theta$ was gridded from 0 to 1.0 with a spacing of 0.1, but with the additional value $\cos[(0.5\cos^{-1}(0.9)]$ (12 values). The impact parameter b was gridded for the most part at a spacing of 0.2 bohr, although we used a spacing of 0.1 bohr at small impact parameters in several cases, resulting in a total of from 25 to 31 values of b at each energy. The range of b was from 0.4 or 0.5 bohr to large enough values to ensure that all scattering through angles larger than 2.5° was included. The calculations for HD were done as two separate cases, with H and D interchanged.

The trajectories were calculated by numerical integration of Hamilton's equations expressed in terms of the three Cartesian components of $\vec{r}$ and $\vec{R}$. The program used a fourth-order Adams-Moulton routine, with a Runge-Kutta-Gill starter.[40] The step size Δt_0 chosen to begin the integration was switched to $\Delta t_0/4$ for R_1 or R_3 less than 3 bohr and then switched again to $\Delta t_0/2$ when R_1 and R_3

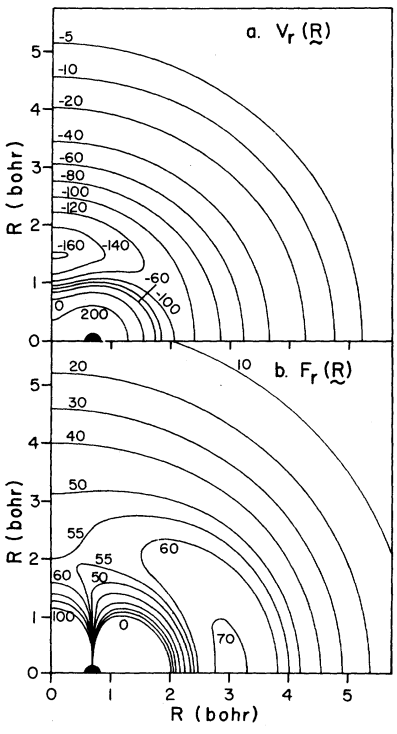

FIG. 1. Contour maps showing features of the H_3^+ potential-energy surface. (a) Potential energy as a function of R and α for a fixed H_2 internuclear separation $r=1.40$ bohr. The contours are labeled in units of 10^{-3} hartree. (b) Component of force along the H_2 internuclear axis as a function of R and α for a fixed H_2 internuclear separation $r=1.40$ bohr. The contours are labeled in units of 10^{-3} hartree/bohr.

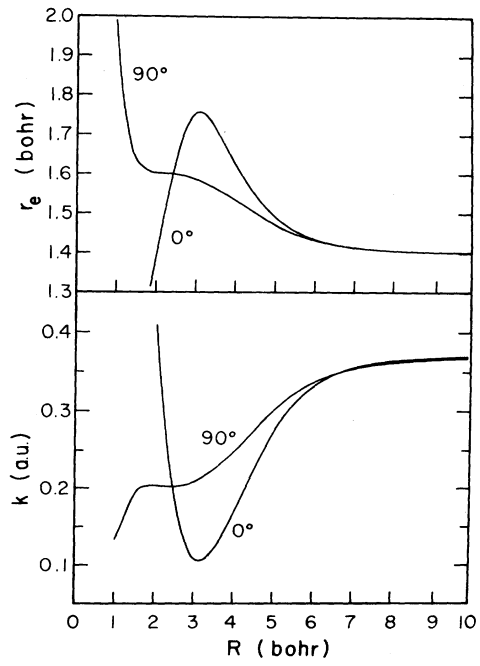

FIG. 2. H_2 equilibrium internuclear distance r_e and vibrational force constant k as functions of proton distance R for the collinear ($\alpha=0°$) and isosceles ($\alpha=90°$) configurations.

became greater than 4 bohr. The accuracy of the integration was tested by backward integrating the calculated trajectories to check for a return to the original starting conditions. This gives a rigorous check on the step size required for accurate integration. We found, however, for a wide variety of initial conditions, that if the calculation conserved energy to sufficient accuracy, it also satisfied the test of backward integration. We therefore simply tested each trajectory for energy conservation, requiring conservation to within 0.002 eV for the 6-eV collisions, and to within 0.005 eV for all the others. This procedure resulted in a numerical value for the vibrational-energy transfer almost always accurate to 0.001 eV. The potential function used is not highly accurate for $r > 2.5$ bohr, and collisions which cause excursions of r beyond this value will therefore not be accurately described by the calculations. However, these cases occur very rarely in the experimental scattering angle regime, and only for small-impact-parameter collisions, which have low probability. Really large increases in r, however, lead to totally erroneous results because the quadrupole moment and polarizability are fitted to cubic functions of r, accurate only for small displacements from equilibrium. We therefore aborted all cases in which r exceeded 10 bohr. The Fortran trajectory-calculation program used an average of about 0.6 sec per trajectory on a CDC 6600 computer.

From each trajectory calculation, we obtain the total molecular internal energy E_T, and the molecular angular momentum L, after the collision. Since the vibrational and rotational motions are coupled, it is necessary to partition the total internal energy into vibrational and rotational degrees of freedom consistently. There is no unique way to do this. We chose to define the rotational and vibrational energies as

$$E_r = L^2/2Mr_m^2, \tag{16}$$

$$E_v = E_T - E_r, \tag{17}$$

where r_m is the separation at the minimum in the effective potential for the centrifugally stretched molecule, and M is the molecular reduced mass.

Monte Carlo averaging

The orientation-averaged differential cross sections in this paper were calculated by interpolation on the grid of values previously obtained, for a large random selection of b, θ, and ϕ. Standard algorithms were used to select properly weighted random values of b and θ.[40]

In a separate calculation, the average transition probabilities as functions of impact parameter were calculated by a Monte Carlo averaging over θ and ϕ at fixed values of b.

The interpolations for E_v, E_r, and χ at each set of random initial conditions (b', θ', ϕ') were done in two steps, using the nine grid values of $(\cos\theta, \phi)$ closest to $(\cos\theta', \phi')$ and the four grid values of b bracketing b'. First a two-dimensional quadratic interpolation in (θ, ϕ) was done for each grid value of b, then a one-dimensional cubic interpolation in b was performed using those four values.

If any of these 36 grid values corresponded to a trajectory calculation which had been aborted because R_2 became too large, a search was made by looping back and decentering the set of grid values used, to attempt to find a complete set of good grid points which would allow an interpolation. If no complete set of good grid values could be found or if the interpolated internal energy exceeded 4.75 eV, the vibrational transition probabilities for that collision were set equal to zero. Otherwise, the probabilities were determined from Eq. (6), in which the quantum-level spacing was taken to be the energy of the $(0 \rightarrow 1)$ transition: 0.516 eV for H_2, 0.450 eV for HD, and 0.371 eV for D_2.

The speed with which the interpolations could be performed (about 500 times as fast as a complete trajectory calculation) enabled us to use a random set of 400 000 initial conditions for each of the four $H^+ + H_2$ calculations, the $H^+ + D_2$ calculation, and each of the two cases in the $H^+ + HD$ calculation. Consequently, the statistical uncertainty in the averaged results is very small—usually less than the linewidth in the plots.

RESULTS AND DISCUSSION

Trajectories

The 31 980 trajectories calculated in this study contain an overwhelming amount of detailed information on the variation of vibrational and rotational excitation energy with initial conditions, which we cannot fully convey here. An examination of some individual trajectories is nevertheless highly valuable in understanding the mechanism of inelastic scattering and in interpreting the features of the averaged quantities. In order to impart some of the flavor of the individual trajectory results, we show in Figs. 3–5 the variation with impact parameter of the polar scattering angle and the vibrational and rotational excitation energies for 10-eV $H^+ + H_2$ collisions and six representative initial molecular orientations, specified as (θ, ϕ) in degrees.

In Fig. 3(a), the polar-angle deflection functions are plotted. The deflection functions each show the expected rainbow maximum in the angle range 22°–29° for impact parameters of 2.6–3.3 bohr.

As the impact parameters are decreased the deflections pass through minima and then rise sharply as the trajectories begin to explore the hard repulsive core of the potential. For the orientation (90, 90), or for any initial molecular orientation in the xz plane, e.g., (0, 0) and (90, 0), the azimuthal scattering angle is required by symmetry to be zero, the deflection function goes to $\chi = 0$, and $\chi(b)$ has a cusp at this point. For nonsymmetric orientations, the x and y components of the deflection are not in general zero simultaneously. Therefore χ passes smoothly through a finite minimum, giving rise to a second classical rainbow, in this case at about half the first rainbow angle. This classical phenomenon will exist for scattering from any anisotropic potential,[22] and is not related to the quantum interference maxima sometimes called "supernumerary rainbows" which appear on the small-angle side of the classical rainbow angle for spherical-potential scattering.

In this range of impact parameter, the scattering is dominated by the valence interaction, not by the long-range terms in the potential. The strongly attractive branch of the valence potential has its longest range in R for the collinear configuration ($\alpha = 0$). At large values of b in the range shown, the largest scattering angles are found for the orientation (90, 0), since in this case the nuclear configuration is approximately linear at the point of closest approach in the trajectory. Similarly, the orientations (0, 0) and (90, 0) give the smallest deflections for a fixed, large value of b. The rainbow scattering angles, on the other hand, are largest for orientations near (0, 0) and (90, 90), because the trajectories for these orientations pass through the isosceles configuration ($\alpha = 90°$), where the potential well is deepest.

The effect of orientation averaging on the angular distribution can be seen in Fig. 3(b), which shows a contour map of the deflection probability distribution function $P_\chi(\chi, b)$. The basic features of this probability distribution became clear upon comparison with the individual deflection functions in Fig. 3(a). The region of highest rainbow-angle probability is indicated by the ridge at $\chi \sim 27.5°$, $b \sim 2.6$ bohr. Local islands of maximum probability are seen at 12.5°, 1.75 bohr, the region in which many of the second rainbow extrema for specific orientations are found, and at 23°, 3.3 bohr, where there is an accidental confluence of the deflection functions for a large number of orientations. The (full width at half-maximum) range of impact parameters which contribute to scattering at fixed χ is typically 0.5 bohr, which is the equivalent of 15 quanta of orbital angular momentum (partial waves). The quantum interference effects should therefore be highly quenched by orientation averaging of the anisotropic potential. The interfer-

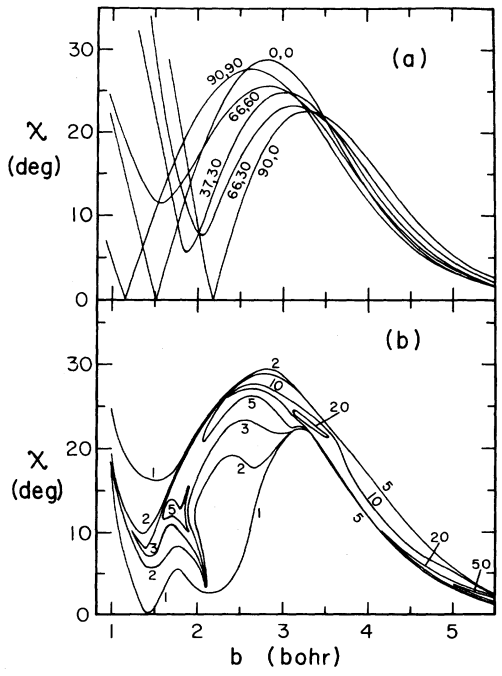

FIG. 3. Polar-angle deflection functions for 10-eV $H^+ + H_2$ collisions and several initial molecular orientation angles (θ, ϕ) in degrees. (b) Contour maps of the polar-scattering-angle probability distribution at fixed impact parameter for 10-eV $H^+ + H_2$ collisions. The numerical values give the percent probability for scattering into a $\frac{1}{2}°$ increment in χ.

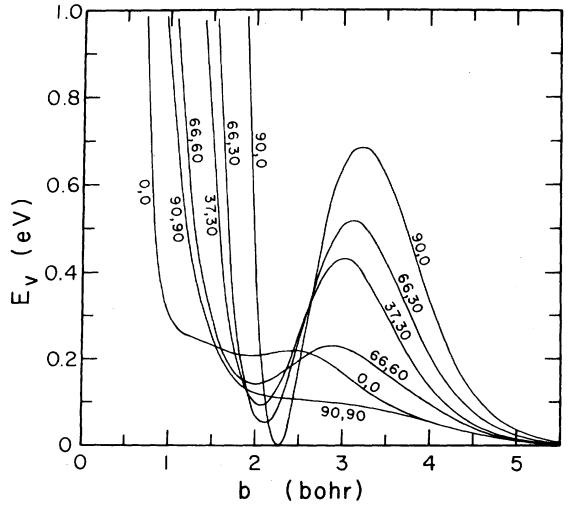

FIG. 4. Classical vibrational-energy transfer as a function of impact parameter for 10-eV $H^+ + H_2$ collisions and several initial molecular orientation angles (θ, ϕ) in degrees.

ence structure in the elastic differential cross section is in fact observed experimentally to have an amplitude approximately an order of magnitude smaller for $H^+ + H_2$ than for $H^+ + Ar$ under similar conditions.[42]

Figures 4 and 5 show the dependence on impact parameter of the vibrational and rotational excitation energies for the same set of representative initial orientations. At impact parameters sufficiently small that the trajectory encounters the hard repulsive potential core, both the vibrational and rotational excitations become very large. In fact, such collisions lead to dissociation of the molecule at impact parameters only slightly smaller than those shown. These small-b encounters also usually result in large scattering angles and are therefore not weighted highly in the experiments. The impact-parameter range most important for scattering in the experimental angle regime runs from about 2 to 5 bohr. It might have been expected that the excitation energy would monotonically increase with decreasing impact parameter, but instead, both the vibrational and rotational energies are generally peaked in this range, with the average vibrational energy about an order of magnitude greater than the average rotational energy. Those initial orientations for which the vibrational energy is strongly peaked show a remarkable correlation between the value of the impact parameter at the maximum vibrational energy and the value of the impact parameter at the rainbow maximum in the angular distribution. Furthermore, at large impact parameters, the vibrational excitation energies for the various initial orientations scale in the same order as the scattering angles for the same orientations. This implies that the radial component of force (along $\vec{R}$) is highly correlated under these conditions with the component of force in the vibrational coordinate (along $\vec{r}$)—a consequence of the fact that the same valence interaction is responsible for both forces. This correlation can easily be seen in Fig. 1. The molecular stretching force is generally a maximum for R values of 2.5–3 bohr, where the potential gradient along $\vec{R}$ is also a maximum. This correlation does not, however, hold at small separations for isosceles configurations, and neither the (90, 90) nor the (0, 0) orientations, both of which have approximately isosceles configurations at the distance of closest approach, possess a maximum in the vibrational excitation energy at the rainbow angle.

In order to understand in detail the shapes of the deflection and excitation functions, it is necessary to examine the motion of the nuclei as a function of time for individual trajectories. Since we cannot possibly describe in detail a number of trajectories large enough to represent the scattering in this system, we instead present information for three special cases in Fig. 6, which illustrate the general nature of the dynamical events taking place. The initial orientation (90, 0) and impact parameters of 2.2, 3.4, and 4.6 bohr were chosen because of the dramatic change in both the vibrational and rotational excitation energies with a change in the impact parameter in this range.

At the impact parameter 4.6 bohr [Fig. 6(c)], the relationship between the vibrational motion $r(t)$ and the force function $F(t)$ can be easily seen. As the force builds up, the H_2 molecule begins to stretch, reaching a maximum extension of 1.62 bohr at time A, after the force has peaked. The decrease in the vibrational force constant during the interaction is responsible for the relatively small curvature in $r(t)$ at small values of R, compared to the vibrational motion of the isolated molecule seen at large R. The maximum excursion in r occurs before the driving force has decayed to zero, therefore between times A and B the force opposes the vibrational motion, leaving the molecule somewhat less excited than it would have been if the force had terminated abruptly at time A.

At an impact parameter of 3.4 bohr [Fig. 6(b)], the driving force acts over essentially the same time period, but has a magnitude about twice that in the collision at 4.6-bohr impact parameter. A fixed-frequency harmonic oscillator, according to Eq. (10), would therefore gain about 4 times the vibrational energy in this case. The actual vibrational excitation energy, however, is a factor of 7 higher for the collision at 3.4-bohr impact pa-

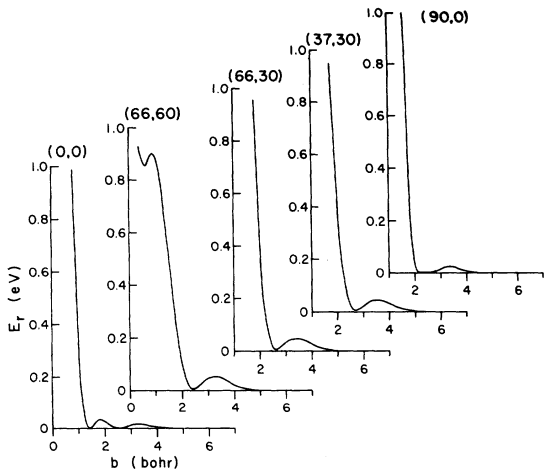

FIG. 5. Classical rotational-energy transfer as a function of impact parameter for 10-eV $H^+ + H_2$ collisions and several initial molecular orientation angles (θ, ϕ) in degrees.

rameter. The difference is due largely to the potential anharmonicity. Because the value of r reaches a larger maximum value in the 3.4-bohr collision, the period of the oscillation is larger and the maximum excursion occurs later in time. A greater fraction of the stretching force is therefore synchronized with the outgoing branch of the oscillator motion—adding to, rather than subtracting from, the vibrational excitation.

The collision at 2.2-bohr impact parameter results in very little vibrational excitation despite the strong driving force. Initially the stretching force and the consequent positive acceleration of r are greater than for the larger impact parameters, but in this case the proton passes close enough to the nearest nucleus of the molecule to encounter the repulsive wall of the potential. There are two results. The driving force becomes negative for a brief period, and the vibrational force constant is suddenly increased (see Fig. 2). These effects combine to stop the motion of r abruptly. The second positive branch of the forcing function then acts to remove almost exactly the vibrational energy deposited in the molecule by the first branch. Although this collision is a special case, it serves to illustrate a feature common to many trajectories for this system—the production of small excitation energy in the collision products because of the partial cancellation of strong, counteracting forces, in the same way that a small scattering angle can result from an intimate small-impact-parameter collision if the contributions to the deflection from the attractive and repulsive branches of the potential just cancel. Effects of this type are largely responsible for the structure observed in Figs. 4 and 5, in the variation of vibrational and rotational excitation energy with impact parameter. As a result, the scattering calculations for this system are very sensitive to subtle changes in the potential surface. One should be highly cautious in comparing with experiment the results of calculations performed using a model potential for this system.

The rotational excitation energies also peak in this impact-parameter range. At large separations, the potential-energy surface for H_3^+ favors the isosceles configuration because of the charge-quadrupole term. As R is decreased, however, the polarization and valence contributions become relatively more important, both of which favor the collinear configuration (for $R \gtrsim 2.5$ bohr). Both the polarizability and quadrupole moment of H_2 are strong functions of the internuclear separation. Figure 6 shows the rotational motion of the molecule which results from these applied torques. In each case θ decreases initially because of the charge-quadrupole torque; then as the separation passes through $R \sim 6$–8 bohr, the torque changes sign. Little change in θ occurs until R passes through its minimum value. At $b = 3.4$ bohr, the molecule is caught in a highly extended position as the proton passes, with the result that a large torque in the negative-Y direction acts during the outgoing leg of the trajectory. In the collision at 4.6-bohr impact parameter the larger values of R and the smaller excursion in the H_2 vibrational coordinate combine to reduce the magnitude of the torque at all times and the rotational excitation energy is small. At $b = 2.2$ bohr, the molecule receives a sharp angular momentum impulse in the positive-y direction as R passes through a minimum, which is canceled by the integral of the torque acting as the products separate.

Orientation averaging

A convenient overview of the trajectory results is obtained by examination of the calculated differential cross sections and the vibrational and rota-

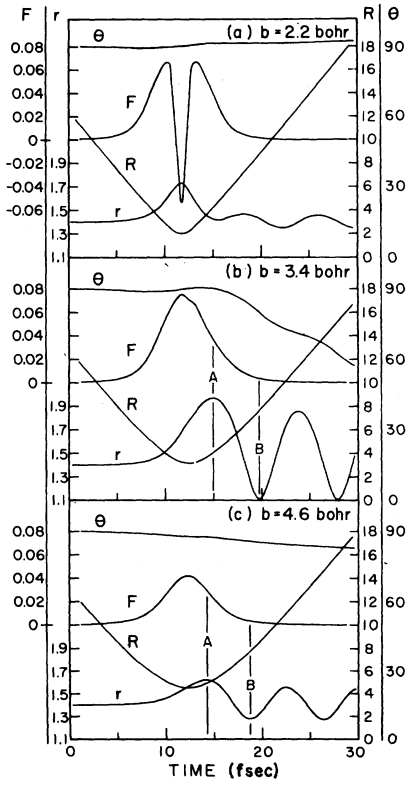

FIG. 6. Salient features of the classical trajectories for 10-eV $H^+ + H_2$ collisions at $\theta = 90°$, $\phi = 0°$ and three different impact parameters: F is the component of force along $\vec{r}$ in hartree/bohr, r is the H_2 internuclear distance in bohr, R is the distance from the proton to the H_2 center of mass in bohr, and θ is the H_2 polar orientation angle in degrees.

tional excitation energies averaged over impact parameter and initial molecular orientation at fixed scattering angle. Figure 7 shows $I(\chi)$, $\overline{E}_v$, and $\overline{E}_r$ as functions of χ for the six cases treated here. Many similarities are apparent. Each of the differential cross sections has a distinct orientation-averaged rainbow maximum, and the second rainbow maximum can be seen except in the two highest-energy calculations. The average vibrational energy peaks sharply in each case near the rainbow angle, coinciding with our previous observation of a correlation between the rainbow angle and the vibration excitation maximum for specific initial orientations. Both the vibrational and rotational energies rise abruptly beyond the rainbow angle, where only the short-range repulsive branch of the deflection function contributes to the scattering.

The average rotational energy seems at first surprisingly large considering the fact that no evidence whatever of rotational excitation was discernible in the experimental data. The measured energy-loss spectra showed peaks for the resolved vibrational states at the energies calculated for pure vibrational transitions. As a comparison of the rotational energies in Figs. 5 and 7(a) indicates, however, most of the contribution to the average rotational energy in the experimental angle range comes not from the large-impact-parameter collisions which dominate the vibrational excitation, but from the collisions at small impact parameters which excite a large number of high-energy rotational states but with very small probability. In the experiments, such rotational excitation will appear as simply a broad background underlying the vibrational structure. Because the small-impact-parameter scattering is relatively isotropic, the average rotational energy does not vary strongly with χ between the two rainbow angles. It does, however, drop off rapidly at angles smaller than the second rainbow angle, since there are no contributions from the repulsive branch of the deflection function, for any given initial orientation, at an angle smaller than the second rainbow angle for that orientation. Postponing for the moment the problem of separating the vibrational and rotational contributions to the experimental energy-loss spectra, a direct comparison of the theoretical and experimental average excitation energies at constant scattering angle can be made. The experimental and theoretical values are given in Table I for all cases in which both the calculations and experiments were performed. Unfortunately, in some cases the experimental energy scans did not cover a sufficient energy range to include all the inelastic scattering. Except for these cases, which are footnoted in Table I, the agreement between theory and experiment is excellent.

There does not appear to be a simple interpretation of the isotope effect on the average vibrational

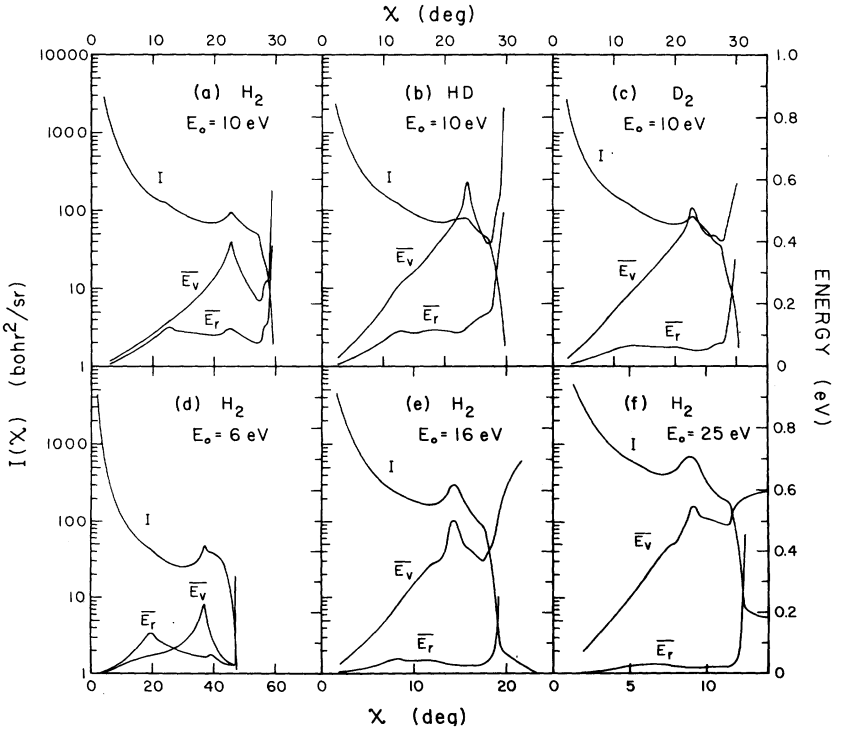

FIG. 7. Classical orientation-averaged differential cross section and vibrational and rotational excitation energies as functions of scattering angle for the indicated relative kinetic energies and target molecule isotopic compositions.

excitation energy. In this energy range, where the forcing function $F(t)$ acts over a time period comparable to a vibrational period, one cannot easily predict the effect of a change in the reduced mass or the vibrational frequency. The smaller rotational excitation of D_2 compared to H_2, however, is simply explained. If the translational and vibrational motion is similar in the two cases, approximately the same torque will be applied to the two molecules. Since the collisions are essentially impulsive as far as the rotational motion is concerned, this will result in a rotational excitation energy which is inversely proportional to the molecular moment of inertia and proportional to the square root of the reduced mass of the colliding species. The rotational excitation of D_2 is therefore approximately 0.55 that of H_2 at the same relative kinetic energy. In HD the moment of inertia is also larger than that of H_2, but the potential is also more anisotropic, because of the displacement of the molecular center of mass from the center of charge. The decrease in rotational excitation with increasing kinetic energy, for peripheral collisions such as these, is due to the decrease in the width of the torque impulse, and has been observed experimentally for highly rotationally inelastic $H^+ + HF$ collisions in this same energy range.[42]

Quantum vibrational transition probabilities

The real test of the DECENT model is its ability to predict the quantum transition probabilities for vibrational excitation. The test is particularly stringent in this case since the direct experimental evidence is to be compared with the results of a completely *ab initio* calculation with no adjustable parameters and no (deliberate) approximations other than the dynamical assumptions of the DECENT model. There is, however, a problem with the interpretation of the experimental data which was not anticipated until the trajectory calculations were performed. The vibrational peaks in the experimental energy-loss spectra were found to be located within experimental error (~0.030 eV) at precisely the energies expected for pure vibrational excitation, placing a fairly small upper limit on the probability of rotational transitions to low-lying excited states. The calculations reveal that, indeed, the probability of excitation to a specific rotational state is usually very small, but that in the "hard" collisions, i.e., those which scatter from the repulsive core of the potential, all final rotational states within a very broad energy band are populated with a high enough probability to make the average rotational energy comparable to the average vibrational energy. The experimental transition probabilities reported in our previous paper were obtained by fitting the peaks in the observed energy-loss spectra to a superposition of Gaussian functions, the areas of which were taken to be proportional to the respective vibrational transition probabilities. In the light of the trajectory calculations, it now appears that associated with each vibrational peak there is a high-excitation-energy tail due to rotational transitions. The tail of each vibrational peak underlies all the higher-energy vibrational peaks and contributes to the measured intensity, but does not result in a shift of the peak energies because the tail is nearly flat. The resulting error is usually small for the lower-energy, high-probability transitions, but is very significant for the higher states, where there are contributions to a small observed intensity from the rotational tails of several lower vibrational states.

Figure 8 shows the calculated probability distribution in classical angular momentum for 10-eV $H^+ + H_2$ scattering at several fixed values of χ. In each case the probability is high for small values of J, and then, at some critical value, plummets several orders of magnitude and remains small and relatively smooth up to high J values. One cannot expect the classical calculation to be valid for small J, but for final rotational quantum numbers large enough for the rotational excitation to be confused with vibrational excitation, the classical calculation should be a reasonable approxima-

TABLE I. Average excitation energies (eV); comparison of theory and experiment.

E_0 (eV)	χ (deg)	$\langle \Delta E \rangle_{\text{expt}}$	$\langle \Delta E \rangle_{\text{Th}}$
		H_2	
6	11	0.079	0.082
6	28	0.117[a]	0.173
6	36	0.164[a]	0.251
10	6	0.058	0.082
10	8	0.105	0.138
10	10	0.206	0.199
10	11	0.222	0.228
10	11	0.255	0.228
10	14	0.277	0.269
10	16	0.354	0.309
10	22	0.378	0.470
16	11	0.378	0.374
		HD	
10	11	0.182[a]	0.306
10	22	0.390[a]	0.584
		D_2	
10	11	0.264	0.262
10	22	0.529	0.513

[a] Experimental energy range probably not sufficient to include all excitation.

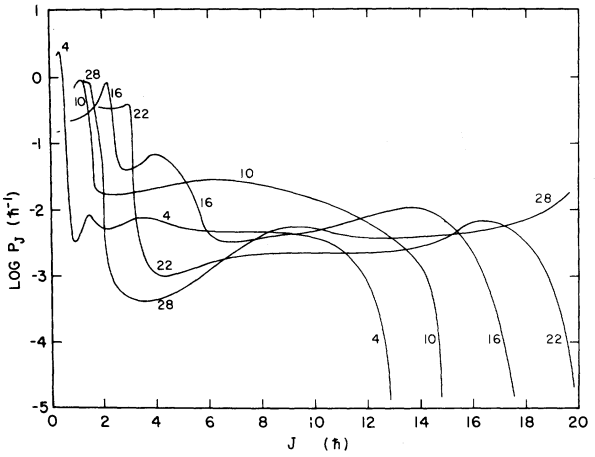

FIG. 8. Probability distribution functions for classical angular momentum transfer in 10-eV $H^+ + H_2$ collisions at fixed scattering angle. The curves are labeled with the scattering angles in degrees.

tion to the quantum rotational transition probability.[41] We have therefore used the rotational-energy distributions at fixed scattering angle from the trajectory calculations to correct the previously fitted experimental transition probabilities for the rotational contributions. First, a Monte Carlo calculation was performed to evaluate the probability of obtaining a final rotational energy within half a vibrational quantum of the energy of each final vibrational level. This calculated rotational distribution was further assumed to be independent of vibrational state. If R_i is the probability of a rotational energy close to the energy of the ith vibrational state and P_n is the (true) probability of the $0 \rightarrow n$ vibrational transition, then the measured probability $\mathcal{P}_n$ of a transition to the nth vibrational-energy bin is

$$\mathcal{P}_n = \sum_{i=0}^{n} P_i R_{n-i} - \sum_{i=n+1}^{\infty} P_n R_{i-n}. \tag{18}$$

From the experimental values of $\mathcal{P}_n$ and the calculated R_i, Eq. (18) can be algebraically inverted to yield the desired values of P_n. The corrected experimental transition probabilities are given in Table II and compared with the DECENT-model calculations in Fig. 9. In each case, the agreement is good to within a reasonable estimate of the experimental uncertainty.

Differential cross sections

The entire set of vibrational-state-resolved differential cross sections calculated in the DECENT approximation is displayed in Fig. 10. The effects of translational energy and of isotopic composition of the target molecule are clear. In each case the rainbow infinity which would result from a spherical scattering potential is smoothed into a broad maximum by the orientation averaging. The small shift of the rainbow maximum to larger scattering angles with increasing final vibrational quantum number, which is observed experimentally, is not

TABLE II. Experimental vibrational transition probabilities corrected for rotational contributions, and comparison with the DECENT-model calculations. (The calculated values are underlined.)

E (eV)	χ (deg)	P_0		P_1		P_2		P_3	
				H_2					
6	28	0.869	0.873	0.172	0.101	0.008	0.018	···	0.005
6	36	0.750	0.713	0.231	0.212	0.041	0.058	···	0.013
10	6	0.960	0.917	0.027	0.074	0.009	0.007	0.005	0.001
10	8	0.923	0.875	0.051	0.109	0.020	0.013	0.008	0.002
10	10	0.794	0.829	0.157	0.144	0.035	0.021	0.012	0.004
10	11	0.766	0.809	0.170	0.160	0.038	0.024	0.018	0.005
10	11	0.788	0.809	0.166	0.160	0.031	0.024	0.010	0.005
10	14	0.683	0.752	0.245	0.200	0.046	0.037	0.017	0.008
10	16	0.577	0.704	0.297	0.227	0.087	0.050	0.025	0.012
10	22	0.507	0.548	0.351	0.291	0.115	0.110	0.024	0.035
16	11	0.517	0.544	0.333	0.318	0.115	0.105	0.029	0.026
				HD					
10	11	0.816	0.667	0.139	0.238	0.036	0.064	0.012	0.019
10	22	0.431	0.407	0.357	0.307	0.189	0.152	0.042	0.069
				D_2					
10	11	0.642	0.606	0.228	0.278	0.084	0.082	0.036	0.023
10	22	0.293	0.313	0.334	0.334	0.231	0.203	0.111	0.093

reproduced by the calculations. The rainbow maxima for vibrationally inelastic scattering tend to be peaked more sharply than those for elastic scattering—a consequence of the fact that the vibrational-energy transfer peaks in this region. The second maximum in the experimental differential cross sections for 10-eV $H^+ + H_2$ scattering is also observed in the calculated differential cross sections. The calculation permits this feature to be identified as the second classical rainbow caused by the potential anisotropy [see Fig. 3(a)].

As in the experiment, the second rainbow is more prominent in the differential cross sections for inelastic scattering, which do not vary as rapidly with angle in this range as does the elastic differential cross section. In the experimental elastic differential cross section, the second classical rainbow is also obscured by the quantum interference structure, which seems to be more effectively averaged out in the inelastic channels. The second rainbow is also visible in the HD and D_2 calculations at 10 eV and in the H_2 calculations at 6 eV.

The experimental and theoretical total differential cross sections [$I(\chi, n)$ summed over all n at each χ] are compared in Fig. 11 for 10-eV $H^+ + H_2$ scattering. The classically calculated function $I(\chi)$ has relatively sharply defined features in the region of the rainbow which one expects to be smoothed over in a quantal calculation in the same way that the classical rainbow infinity for spherical-potential scattering is transformed into a broad maximum. The dashed line in Fig. 11 shows our attempt to estimate the quantum differential cross section near the rainbow maximum semiclassically without computing the semiclassical phase shifts. For spherical-potential scattering, the usual semiclassical expression[43] for the contribution to the differential cross section at the rainbow angle χ_r from the negative branch of the deflection function can be written in terms of the Airy integral as

$$I_r(\chi) = \frac{2\pi l_r q^{-2/3}}{k^2 \sin\chi} \mathrm{Ai}^2(q^{-1/3}(\chi - \chi_r)), \tag{19}$$

in which k is the translational wave number, l is the orbital angular momentum, and q is defined by

$$q = \frac{1}{2}\left(\frac{d^2\chi}{dl^2}\right)_{l_r}. \tag{20}$$

Semiclassically, l may be replaced by the corresponding classical orbital angular momentum (in units of $\hbar$). We applied Eq. (19) to the anisotropic scattering in this case by evaluating $I_r(\chi)$ from the calculated polar-angle deflection function for a given orientation, adding the (small) classical contribution from the repulsive branch, then Monte Carlo averaging the result over initial molecular orientations to obtain $\bar{I}_r(\chi)$. The various contributions to $\bar{I}_r(\chi)$ are therefore not combined coherently as would be required by a rigorous treatment, but since the experiments show no interference structure near the rainbow, this should not be a bad approximation. The semiclassical estimate in

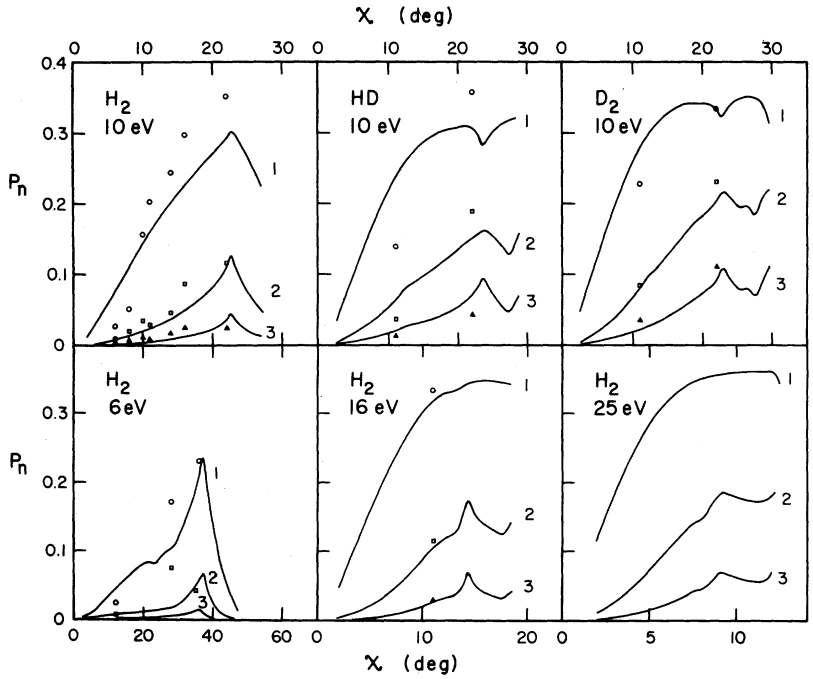

FIG. 9. Quantum vibrational transition probability as a function of scattering angle for the first three excited vibrational states. The solid lines show the results of the DECENT-model calculations and the data points are the experimental values for $n=1$ (○), $n=2$ (□), and $n=3$ (△).

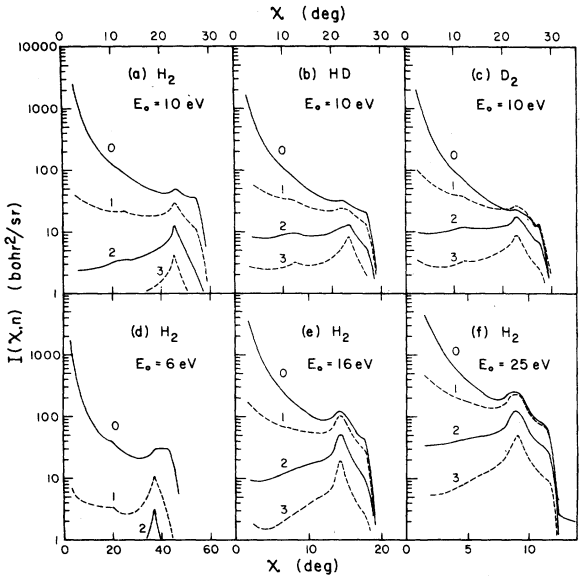

FIG. 10. Calculated differential cross sections as functions of scattering angle for state-resolved vibrational transitions.

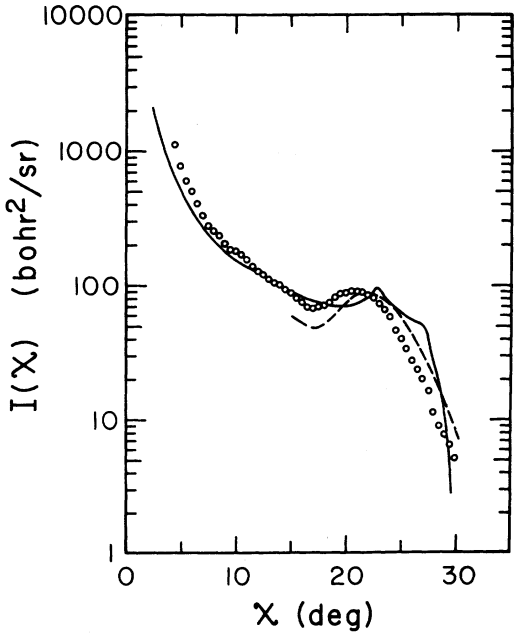

FIG. 11. Comparison of the theoretical and experimental total differential cross sections for 10-eV $H^+ + H_2$ scattering. The solid line shows the orientation-averaged classical differential cross section, the dashed line shows the orientation-averaged semiclassical estimate of the rainbow structure, and the data points are the experimental results, normalized to the classical calculation at $\chi = 15°$.

fact reproduces the shape of the experimental rainbow maximum almost perfectly, but places the maximum at 5% too large an angle. We regard the magnitude of this difference as reasonable, considering the dynamical approximations which are involved, and not an adverse reflection on the accuracy of our potential-energy surface.

Total cross sections

A separate Monte Carlo interpolation calculation was performed to obtain the vibrational transition probabilities averaged over orientation at fixed impact parameter for all six cases. A sample of at least 1000 orientations was used at each impact parameter. The results for the first three excited states are given in Fig. 12. All the curves of P_n versus b have a double-lobed structure consisting of a broad maximum at large b and a relatively

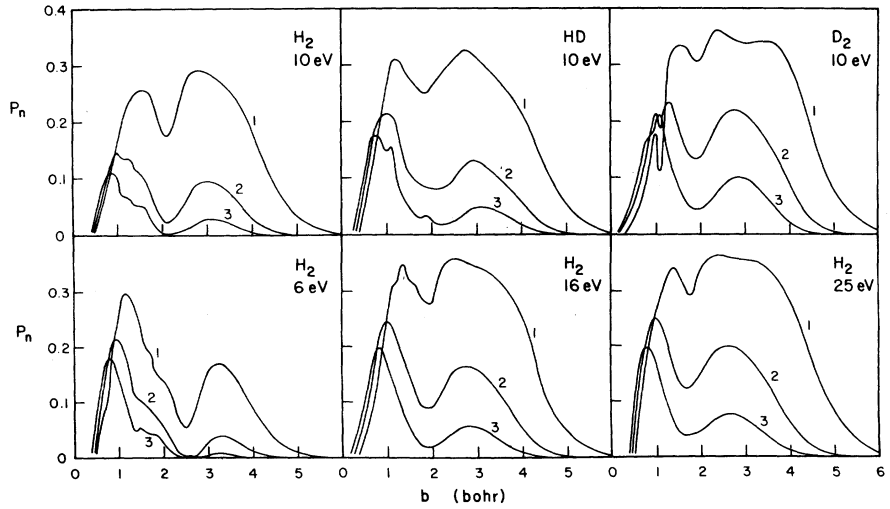

FIG. 12. Orientation-averaged probability for transition to each of the first three vibrationally excited states as a function of impact parameter.

narrow peak at small b. Comparison of Figs. 12 and 4 shows that the large-impact-parameter peak is due mostly to the long-range stretching force while the small-b peak is caused primarily by hard repulsive collisions. The vibrational transition probabilities go to zero for very small b as collisional dissociation becomes the dominant channel. In this energy regime the range of impact parameters which contributes to a particular transition is about the same at all energies, but both the upper and lower cutoffs occur at smaller values of b for the higher-energy excitations.

It is interesting that the contribution to the vibrational excitation cross sections from the large-impact-parameter collisions becomes relatively more important as the kinetic energy is increased. The curves for H_2, HD, and D_2 target molecules have qualitatively similar shapes although they differ in detail because of the different vibrational periods of the three molecules and the greater anisotropy of the $H^+ + HD$ potential.

The total cross sections σ_n for excitation of the first three vibrational states were calculated by numerical integration of the probability functions:

$$\sigma_n = 2\pi \int_0^\infty b P_n(b)\, db\,. \tag{21}$$

The values obtained are listed in Table III. No experimental values of σ_n in this energy range are available for comparison, although Herrero and Doering have performed measurements of integral cross sections for $H^+ + H_2$ and $D^+ + H_2$ vibrational excitation at higher energies.[44] It would be possible to compare the calculations with the experiments of Herrero and Doering if the angular transmission function of their apparatus were accurately known. A much better comparison, however, can be made by direct calculations in the higher-energy regime, which we will report in a later paper. The calculated low-energy total cross sections increase with increasing energy, while the high-energy experimental cross sections for $H^+ + H_2$ decrease with increasing energy above 100 eV. This is consistent with the conclusion of Herrero and Doering that the total cross sections for vibrational excitation peak below 100 eV.

TABLE III. Total cross sections for vibrational excitation (in the DECENT approximation).

System	E (eV)	Cross sections (bohr^2) σ_1	σ_2	σ_3
$H^+ + H_2$	6	8.21	2.37	1.13
	10	14.72	3.77	1.20
	16	20.22	6.84	2.35
	25	22.19	8.26	2.94
$H^+ + HD$	10	17.99	5.99	2.27
$H^+ + D_2$	10	22.27	9.52	3.99

The total cross sections calculated for $H^+ + H_2$ vibrational excitation at 10 eV by Collins, Preston, and Cross[12] are considerably higher than those obtained here. It is not clear whether this is caused by the difference in the dynamical models or by the different potential surface which they used.

CONCLUSIONS

The DECENT model is capable of providing quantitatively useful predictions of the quantum transition probabilities for vibrational excitation in molecular collisions, using dynamical calculations which are purely classical. In the case of small-angle $H^+ + H_2$ scattering at ~10-eV energy, the calculations clearly show that vibrational excitation is caused principally by "bond dilution"—the weakening and stretching of the H_2 bond as electron density is temporarily withdrawn by the passing proton. All initial molecular orientations contribute comparably to the vibrational excitation. In the $H^+ + H_2$ example treated here, it would be a poor approximation, for any individual trajectory, to calculate the classical vibrational-energy transfer using Eq. (10), in which $F(t)$ is evaluated at a fixed H_2 internuclear separation and the Fourier component calculated at the original harmonic-oscillator frequency. A partial cancellation of errors may, however, result from averaging over initial conditions.

The maximum which appears in the experimental inelastic differential cross sections at about half the rainbow angle is revealed by the trajectory calculations to be associated with the orientation-averaged second classical rainbow, caused by the anisotropy of the potential.

Although the probability of rotational transitions to any particular final excited state is small, the sum of all such transitions results in an average rotational excitation energy which is not negligible, as had been previously assumed. It is therefore necessary to correct the experimental vibrational transition probabilities for contributions from small-probability, high-energy rotational excitations. Once the corrections are made, the agreement between the DECENT model and the experimental vibrational transition probabilities is very satisfactory.

ACKNOWLEDGMENTS

During the course of this work, the authors enjoyed the benefit of many helpful discussions with Professor Donald G. Truhlar and Professor S. E. Buttrill, Jr.

†Research supported in part by the National Science Foundation under Grants No. GP-14410 and GP-38759x, and by a grant from the University of Minnesota Computer Center.

[1]H. Udseth, C. F. Giese, and W. R. Gentry, Phys. Rev. A 8, 2483 (1973). A bibliography of other experimental measurements is given in this paper, but is not duplicated here; also H. Udseth, C. F. Giese, and W. R. Gentry, J. Chem. Phys. 54, 3642 (1971).

[2]D. Secrest, Ann. Rev. Phys. Chem. 24, 379 (1973).

[3]D. Rapp and T. Kassal, Chem. Rev. 69, 61 (1969).

[4]K. Takayanagi, Prog. Theor. Phys. Suppl. 25, 1 (1963).

[5]W. Eastes and D. Secrest, J. Chem. Phys. 56, 640 (1972); P. McGuire and D. A. Micha, Int. J. Quantum Chem. 6, 111 (1972); J. Schaeffer and W. A. Lester, Chem. Phys. Lett. 20, 575 (1973); J. Chem. Phys. 59, 3676 (1973); 60, 1672 (1974).

[6]D. J. Locker and D. J. Wilson, J. Chem. Phys. 52, 271 (1970).

[7]M. A. Wartell and R. J. Cross, J. Chem. Phys. 55, 4983 (1971).

[8]P. Pechukas and J. P. Davis, J. Chem. Phys. 56, 4970 (1972).

[9]A. P. Penner and R. Wallace, Phys. Rev. A 9, 1136 (1974).

[10]B. Ritchie, Phys. Rev. A 6, 1902 (1972).

[11]R. J. Gordon and A. Kuppermann, J. Chem. Phys. 58, 5776 (1973).

[12]F. S. Collins, R. K. Preston, and R. J. Cross, Chem. Phys. Lett. 25, 608 (1974).

[13]For example, W. H. Miller, Acc. Chem. Res. 4, 161 (1971); an extensive bibliography of this work is given in Ref. 2.

[14]J. D. Doll and W. H. Miller, J. Chem. Phys. 57, 5019 (1972).

[15]A. Messiah, *Quantum Mechanics* (North-Holland, Amsterdam, 1966), Vol. 1, Ch. XII.

[16]*ibid.* p. 216

[17]L. D. Landau and E. M. Lifshitz, *Mechanics*, 2nd ed. (Pergamon, New York, 1969).

[18]E. H. Kerner, Can. J. Phys. 36, 371 (1958).

[19]M. S. Bartlett and J. E. Moyal, Proc. Camb. Philos. Soc. 45, 545 (1949); R. P. Feynman, Rev. Mod. Phys. 20, 367 (1948); P. Pechukas and J. C. Light, J. Chem. Phys. 44, 3897 (1966); H. K. Shin, Chem. Phys. Lett. 3, 125 (1969).

[20]The general relation for the probability of the transition $(n \rightarrow m)$ is $P_{mn} = m!\,n!\,e^{-\epsilon}\,\epsilon^{m+n}\,S_{mn}^2$, where $S_{mn} = \sum_{j=0}^{\min(m,n)} [(-1)^j \epsilon^{-j}/(n-j)!\,j!\,(m-j)!]$.

[21]A similar suggestion in the context of the ITFITS model was made by K. Shobatake, S. A. Rice, and Y. T. Lee, J. Chem. Phys. 59, 2483 (1973).

[22]R. J. Cross, J. Chem. Phys. 49, 1976 (1968).

[23]C. E. Treanor, J. Chem. Phys. 43, 532 (1965); 44, 2220 (1966).

[24]A modification of the ITFITS model which permits the treatment of slow collisions involving highly vibrationally excited molecules has been suggested by M. Rubinson, B. Garetz, and J. I. Steinfeld, J. Chem. Phys. 60, 3082 (1974).

[25]H. K. Shin, J. Phys. Chem. 73, 4321 (1969).

[26]K. E. Holdy, L. C. Klotz, and K. R. Wilson, J. Chem. Phys. 52, 4588 (1970).

[27]F. E. Heidrich, K. R. Wilson, and D. Rapp, J. Chem. Phys. 54, 3885 (1971).

[28]R. I. Morse, J. Chem. Phys. 54, 4138 (1971).

[29]B. H. Mahan, J. Chem. Phys. 52, 5221 (1970).

[30]R. K. Preston and J. C. Tully, J. Chem. Phys. 54, 4297 (1971).

[31]I. G. Csizmadia, R. E. Kari, J. C. Polanyi, A. C. Roach, and M. A. Robb, J. Chem. Phys. 52, 6205 (1970); the complete table of potential values was kindly sent to us by Professor Csizmadia and Professor Polanyi.

[32]C. W. Bauschlicher, Jr., S. V. O'Neil, R. K. Preston, H. F. Schaefer III, and C. F. Bender, J. Chem. Phys. 59, 1286 (1973); the complete table of potential values was kindly sent to us by Professor Schaefer.

[33]G. D. Carney and R. N. Porter, J. Chem. Phys. 60, 4251 (1974); G. D. Carney, Ph.D. thesis (University of Arkansas, 1973) (unpublished).

[34]W. Kolos and L. Wolniewicz, J. Chem. Phys. 46, 1426 (1967).

[35]D. G. Truhlar, Int. J. Quantum Chem. 6, 975 (1972); W. Kolos and L. Wolniewicz, J. Chem. Phys. 43, 2429 (1965).

[36]The influence of varying the analytic form, and the criterion for best fit, on calculations of vibrational excitation in the system He + H_2, has been discussed by M. H. Alexander and E. V. Berand, J. Chem. Phys. 60, 3950 (1974).

[37]H. M. Hulburt and J. O. Hirschfelder, J. Chem. Phys. 9, 61 (1941). The subject of empirical potential functions for simple molecules has been reviewed by D. Steel, E. R. Lippincott, and J. T. Vanderslice, Rev. Mod. Phys. 34, 239 (1962).

[38]J. Korobkin and Z. I. Slawsky, J. Chem. Phys. 37, 226 (1962).

[39]H. J. Loesch and D. R. Herschbach, J. Chem. Phys. 57, 2038 (1972).

[40]D. L. Bunker, *Methods in Computational Physics*, edited by B. Alden, S. Fernbach, and M. Rotenburg (Academic, New York, 1971), pp. 287–325. In Eq. 41, −1475 should be replaced by +1427.

[41]See, for example, R. A. LaBudde and R. B. Bernstein, J. Chem. Phys. 59, 3687 (1973).

[42]H. Udseth, C. F. Giese, and W. R. Gentry, J. Chem. Phys. 60, 3051 (1974).

[43]R. B. Bernstein, *Advances in Chemical Physics*, edited by John Ross (Wiley, New York, 1966), Vol. X, p. 103.

[44]F. A. Herrero and J. P. Doering, Phys. Rev. A 5, 702 (1972).